

AIRCRAFT OBSERVATIONS OF A COASTALLY TRAPPED WIND REVERSAL OFF THE CALIFORNIA COAST

David A. Rahn *

University of Wyoming, Laramie, Wyoming

1. INTRODUCTION

During summertime months the low-level airflow over the eastern Pacific is dominated by the circulation associated with the Pacific High typically situated about 1000 km off the west coast of the United States. Subsidence above the Pacific High establishes a sharp temperature inversion at the top of the well-mixed marine boundary layer (MBL) with its depth increasing offshore to the west. A low-level coastal jet (CJ) is commonly found embedded within the broad northerly winds in response to this sloping inversion (e.g., Burk and Thompson 1996). The northerly wind regime is disrupted at times by coastally-trapped wind reversals (CTWRs, also referred to as coastally trapped disturbances or southerly surges) characterized by southerly wind and fog or stratus adjacent to the coastline that extends westward about 100 km (e.g., Ralph et al. 1998 and Nuss et al. 2000).

Propagating CTWRs have a common synoptic signature as described in Mass and Bond (1996) and Nuss (2007). From nearly zonal geopotential heights at 500 hPa, a ridge over the eastern Pacific amplifies and tracks slowly to the east. The surface high tends to strengthen about two days before the event and track northeast while the existing trough over central California amplifies toward the coast. Low-level offshore flow develops advecting the warm continental air offshore, which is further warmed as it subsides down the elevated coastal topography. As a result, the MBL is lowered and this is often associated with a fairly weak horizontal pressure gradient force (PGF) near the coast.

A number of conceptual models of CTWRs have been proposed, but the primary mechanism that causes and maintains this reversal is not currently widely accepted. Coastal mountains with heights about 300-800 m exist along the west coast with varying topographic features including a significant gap near San Francisco. The terrain is generally above the MBL, providing a vertical boundary. This two-layer system with a lateral

boundary may support a variety of classes of air motions (Burk and Thompson, 2004).

A review of the proposed conceptual models is discussed in Nuss et al. (2000). These events have been interpreted as Kelvin waves, topographically trapped density currents, internal bores, and as a response to a synoptically driven pressure gradient reversal that produces a trapped ageostrophic response. It has also been proposed that a combination of forcing forms and regulates the CTWR, so that it is controlled by both marine layer processes and also synoptic forcing.

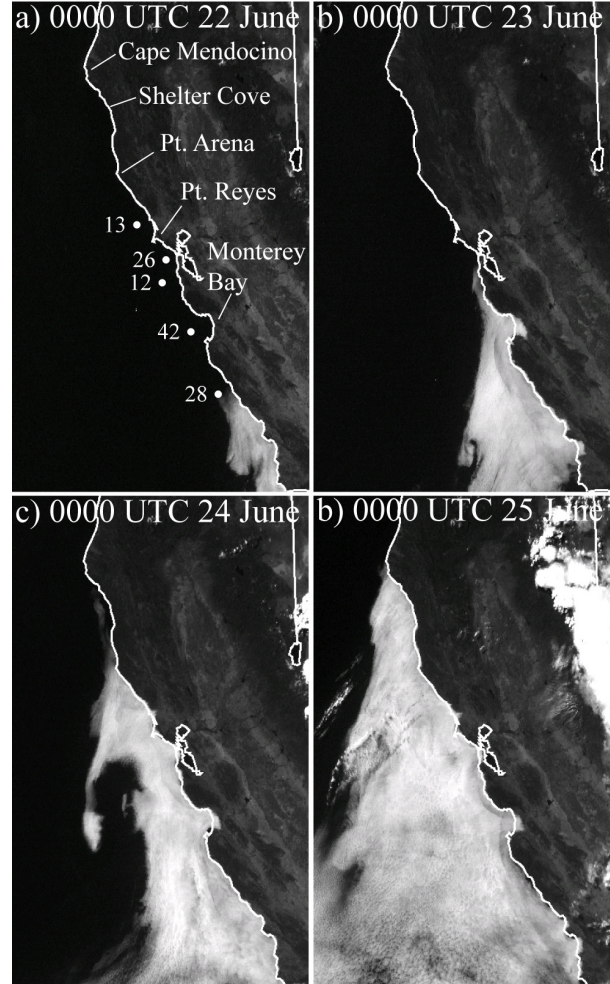


Fig. 1: Visible satellite imagery at 0000 UTC on (a) 22 June 2006, (b) 23 June 2006, (c) 24 June 2006, and (d) 25 June 2006. Significant geographic sites and buoy locations indicated in (a).

* *Corresponding author address:* David A. Rahn, Univ. of Wyoming, Dept. of Atmos. Sci., Laramie, WY 82071; e-mail: darahn@uwyo.edu

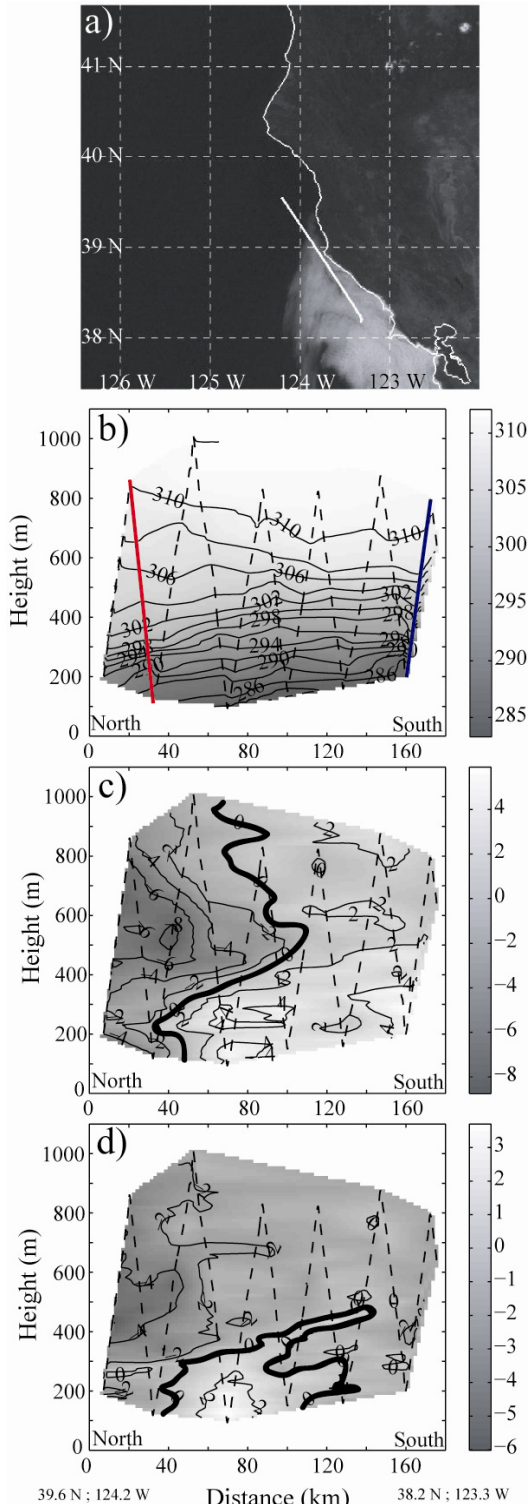


Fig. 2: Sawtooth leg 1645 to 1726 UTC on 23 June 2006 showing (a) visible satellite image at 1700 UTC overlaid with flight track, (b) potential temperature (K, solid and grayscale), (c) along-shore wind speed (m s^{-1} , solid and grayscale), and (d) cross-shore wind speed (m s^{-1} , solid and grayscale). Bold line indicates zero contour and dashed line is the flight track.

While there have been studies utilizing both observational data such as sounder and buoy data, and also numerical simulations, few in-situ airborne measurements of CTWRs exist. This was in part motivation for the Dynamics and Microphysics in Marine Stratocumulus (DMIMS) field project conducted in May and June 2006 and based in Arcata, CA. During this field campaign, one strong CTWR event occurred and was documented during the propagating and the decaying phases. Aircraft observations of the propagating stage of this CTWR are presented here to characterize this CTWR event. Attention is given to the structure of the observed MBL, winds, and PGF and their implications. The second section describes the event and the synoptic conditions and includes a brief discussion of the aircraft measurement techniques. The third section describes the key aircraft observations in detail and their implications. The final section presents a summary and the conclusions.

2. EVENT OVERVIEW AND METHODS

The CTWR event of 22-25 June 2006 was a strong propagating event. The evolution and progression northwards along the California coast is shown by visible satellite imagery in Fig. 1, which also includes significant geographic sites and buoy locations. Initiation took place near Point Conception. It traveled along the coast with an eddy developing southwest of Point Arena on the morning of 23 June. It continued north until it stalled on the south side of Cape Mendocino and eventually decayed.

Synoptic features in this case were typical for a propagating event as described in Mass and Bond (1996) and Nuss (2007). The Pacific High tracked to the northeast late on 20 June and this supported strong and persistent low-level offshore flow across the entire west coast, a necessary feature for propagating CTWRs. The offshore flow implies warm air advection off the continent and subsidence as the air moves down the coastal ranges. The PGF became fairly weak along the coast south of Cape Mendocino.

This CTWR event was explored by the University of Wyoming King Air (UWKA) research aircraft during DMIMS to document the characteristics of the wind reversal. The morning flight and the afternoon flight on 23 June that document a CTWR during its propagating stage are presented. At the time of the observations, the leading cloud edge is located near Point Arena. Flight strategies include sawtooth maneuvers to measure the vertical structure of the CTWR and

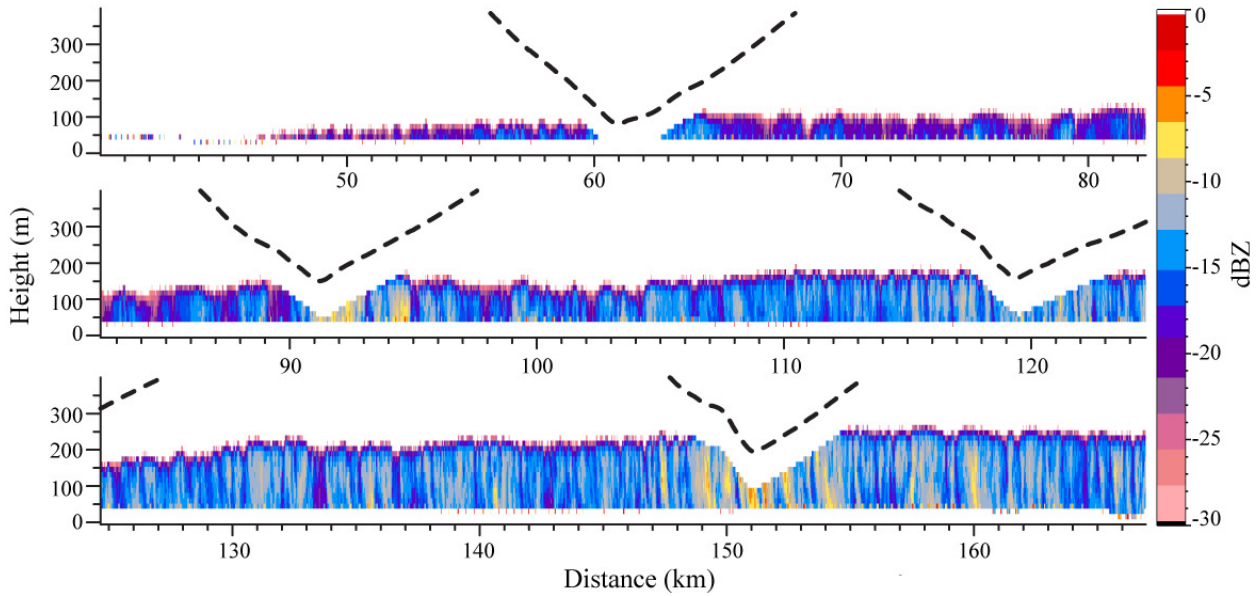


Fig. 3: Reflectivity (dBZ) derived from the WCR from the alongshore sawtooth leg 1645 to 1726 UTC 23 June 2006 using the same distance scale as Fig. 2. The dashed black line indicates the aircraft path and the notches in reflectivity are due to the ~ 125 m dead-zone of the WCR.

isobaric legs to directly measure the height of the isobaric surface. Extremely accurate height measurements that are necessary to calculate the small isobaric slope are obtained using both radar altimetry and differential GPS, which are in good agreement. Deviations off of the isobaric surface are corrected hydrostatically. This provides a direct measurement of the component of the PGF that is along the flight path. A detailed discussion of this method is provided in Parish et al. (2007) and a recent application of this method is provided in Rahn and Parish (2007).

Numerous legs were conducted in both alongshore and cross-shore directions over various scales with the cross-shore sampling reaching as close as 10 km to the shoreline. The wind is decomposed into alongshore and cross-shore wind components, which are defined by 330° and 60° , respectively. This is done since the coastline is roughly represented by this direction. When examining the individual flight legs, the horizontal position is defined by the distance from the northernmost or westernmost point of the flight track, so that either north or west is on the left side of the figure. The UWKA also had remote sensing capabilities since the Wyoming Cloud Radar (WCR) was operating during these flights. This aided in understanding the nature of the low-level cloud layer since the UWKA could not fly at those low levels for long durations. Technical information regarding the WCR can be found in Leon et al. (2006) and at <http://www-das.uwyo.edu/wcr/>.

3. OBSERVATIONS

The first leg on 23 June 2006 was an alongshore sawtooth pattern that documented the vertical structure of the MBL. The flight leg was centered at the leading cloud edge near Point Arena, Fig. 2a. The MBL is represented by potential temperature contours, Fig. 2b. These contours slope upward to the south, implying a deeper and cooler MBL to the south without much change in the stability. Over this leg the inversion layer is not shallow above the well-mixed layer below, but rather deep and has a more or less uniform vertical gradient in the potential temperature between about 250 and 500 m. This deepening and cooling of the MBL to the south is associated with a PGF directed to the north. The PGF can be estimated from these soundings. While not as accurate as the 996-hPa redundant isobaric legs conducted subsequently, a 996-hPa isobaric surface was interpolated from this leg to calculate the approximate PGF. The estimated northward PGF corresponds to an onshore geostrophic wind component of $\sim 2 \text{ m s}^{-1}$. This northward PGF is also confirmed by more accurate alongshore 996-hPa isobaric legs (not shown) corresponding to an onshore geostrophic wind of 8 m s^{-1} . Alongshore and cross-shore wind components during the first leg are depicted in Figs. 2c and 2d, respectively. The bold line indicates the zero contour. The alongshore wind

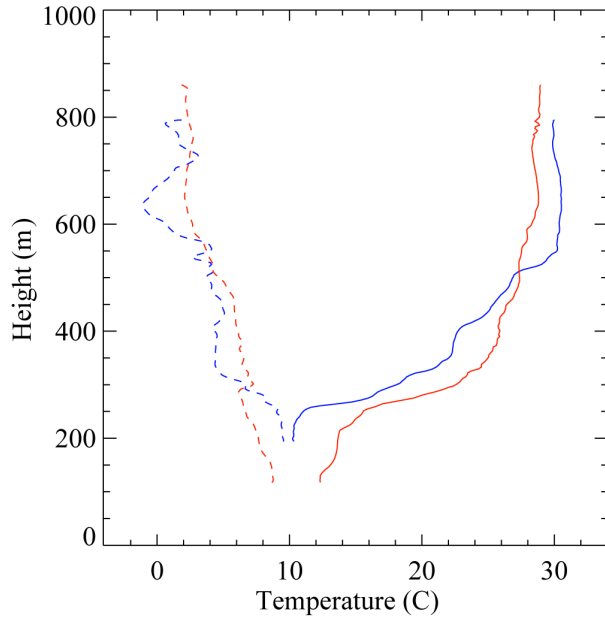


Fig. 4: Profiles of temperature (C, solid) and dewpoint temperature (C, dashed) from the first sawtooth leg. Locations of the north (red) and south (blue) locations are indicated Fig. 2.

reversal is captured by this flight leg. Maximum observed southerly wind is above 4 m s^{-1} . The alongshore wind also tends to be consistent with the MBL structure. Light cross-shore wind is found throughout the leg with a maximum onshore component over 2 m s^{-1} just north of Point Arena ($\sim 80 \text{ km}$). This onshore flow is most likely due to the southerly flow rounding the point. The important feature of the wind components is that the total wind is orientated primarily alongshore.

The UWKA could not extensively examine the cloud layer directly since it was quite shallow, and would pose flight safety concerns. However, cloud properties including cloud-top height and structure were derived from this first sawtooth using the WCR reflectivities, Fig. 3. A thin fog layer begins at the surface near Pt. Arena ($\sim 50 \text{ km}$) and increases to a height of $\sim 250 \text{ m}$ just northwest of Pt. Reyes. This mimics the general increase of the MBL depth to the south shown in Fig. 2b. Little vertical wind shear can be inferred from these reflectivity images and this is confirmed by an analysis of the horizontal dual Doppler velocities (not shown). Because the WCR reflectivities indicate fairly uniform vertical reflectivities, not a maximum near the top that would be associated with condensational growth of cloud droplets, this suggests that drizzle is present and dominating the reflectivity. There is some small-scale structure to the clouds in the form of regions of enhanced

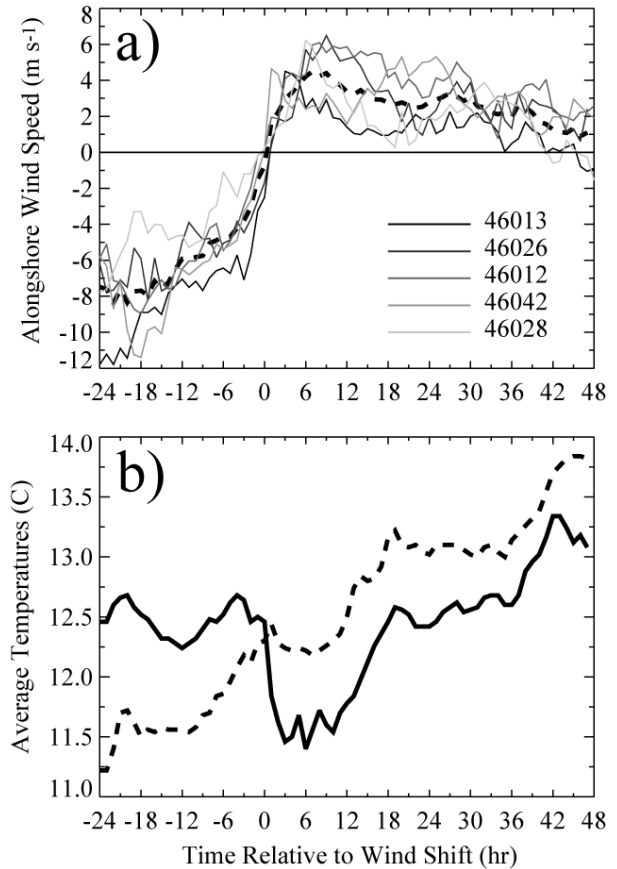


Fig. 5: Individual (thin) and average (thick) of all buoy observations relative to the time of the wind reversal including (a) alongshore wind component (m s^{-1}) and (b) air (solid) and water (dashed) temperatures (C).

reflectivity and variations of cloud-top height, which may be difficult to see from this exaggerated aspect ratio.

Two soundings taken from the previous sawtooth leg (locations indicated in Fig. 2b) highlight differences between the environment north and south of the cloud head, Fig. 4. The northern sounding (red) indicates that the strong inversion base is near 250 m. Under this strong inversion, the temperature does continue to cool somewhat nearing the surface, indicating a fairly stable layer under the strong inversion. The southern sounding (blue) also has a strong inversion base near 250 m, but at any given height below $\sim 450 \text{ m}$ the southern sounding is about 3 C cooler than the northern sounding. This highlights the density difference between the two regions. While the southern sounding does not reach as far to the ground due to the presence of the cloud, it can be inferred that this region is less stable than the area to the north. This is mainly due to the cloud top radiational cooling.

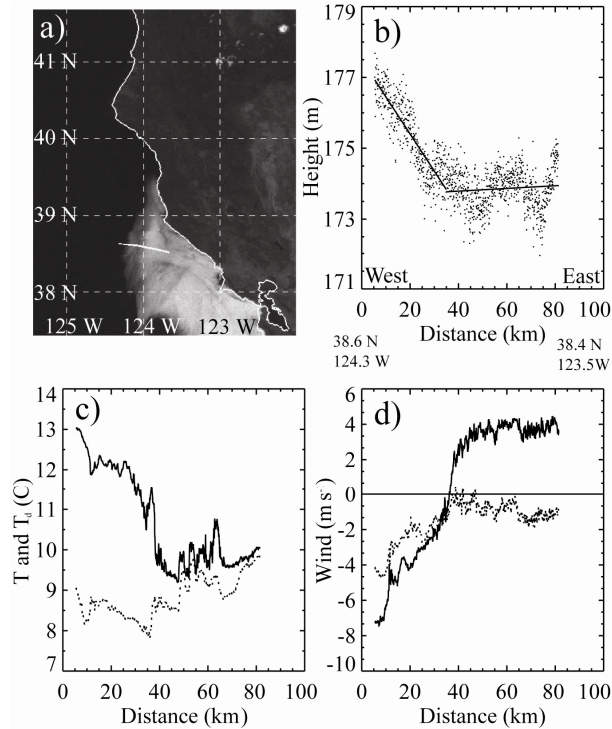


Fig. 6: Isobaric leg at 998 hPa from 1855 to 1914 UTC 23 June 2006 showing (a) visible satellite image at 1915 UTC 23 June 2006 overlaid with flight track, (b) height (m) and linear regression lines, (c) temperature (solid) and dew point (dashed) temperature (C), and (d) alongshore (solid) and cross-shore (dashed) wind speed (m s^{-1}).

Buoy observations relative to the time of the reversal also illustrate the density difference as the CTWR progresses up the coast. The average alongshore wind component (thick dashed line) in Fig. 5a demonstrates the weakening of the northerly wind in the 24 hours prior to the actual reversal and the light, but persistent, southerly wind in the 48 hours after the reversal. Figure 5b shows that prior to the wind reversal, the air temperature (solid line) is warmer than the water temperature (dashed line). After the wind reversal a 1 C drop in the average air temperature occurs. The water temperature increases over the entire time period due to the absence of upwelling. This results in the air temperature being about 0.5 C colder than the water temperature during the 48 hours after the reversal.

A 998-hPa isobaric leg south of the wind reversal, Fig. 6a, examines the cross-shore characteristics and documents the transition from the northerly CJ in the west to the southerly surge near the coast that occurs near ~40 km. The height of the 998-hPa isobaric surface, Fig. 6b, shows a clear transition from the strong eastward

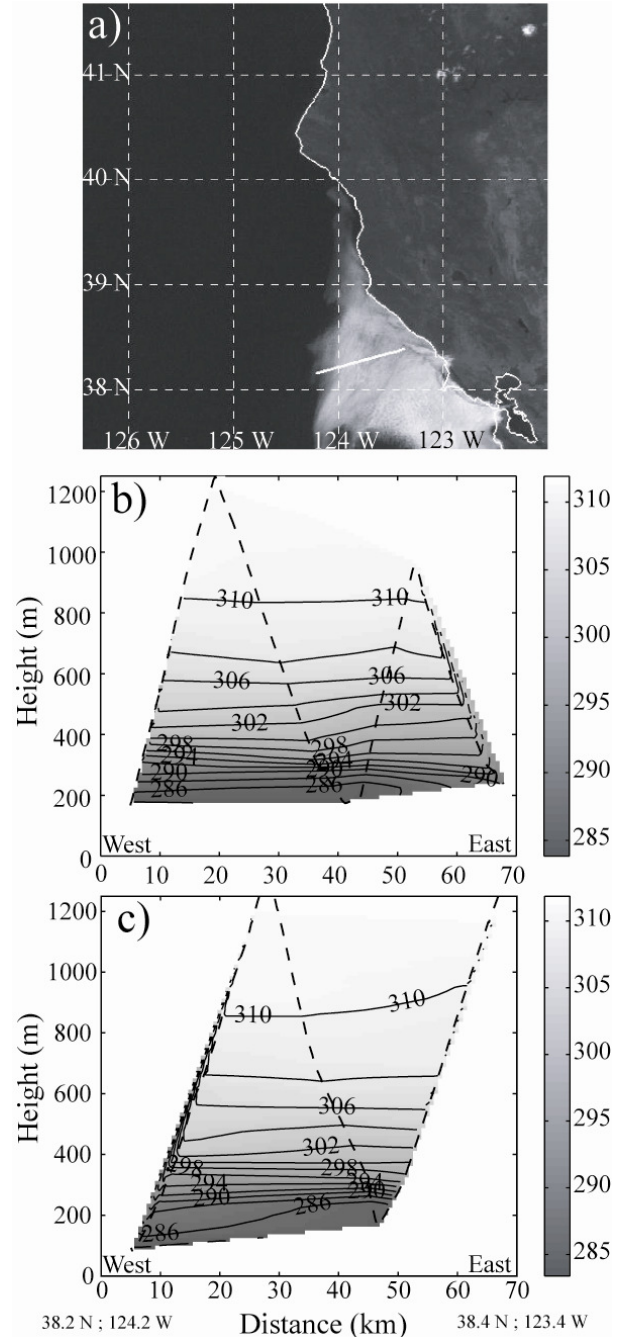


Fig. 7: Sawtooth leg from 2103 to 2118 UTC on 23 June 2006 showing (a) visible satellite image at 2130 UTC 23 June 2006 overlaid with flight track, (b) potential temperature (K, solid and grayscale) with flight track overlaid (dashed), and (c) as (b) but for the return flight 2129 to 2143 UTC.

PGF component to the minimal cross-shore PGF component located within the southerly surge. The western portion of the leg has an associated geostrophic wind from the north at 11 m s^{-1} , while the alongshore geostrophic wind is near zero within the wind reversal. This transition is also

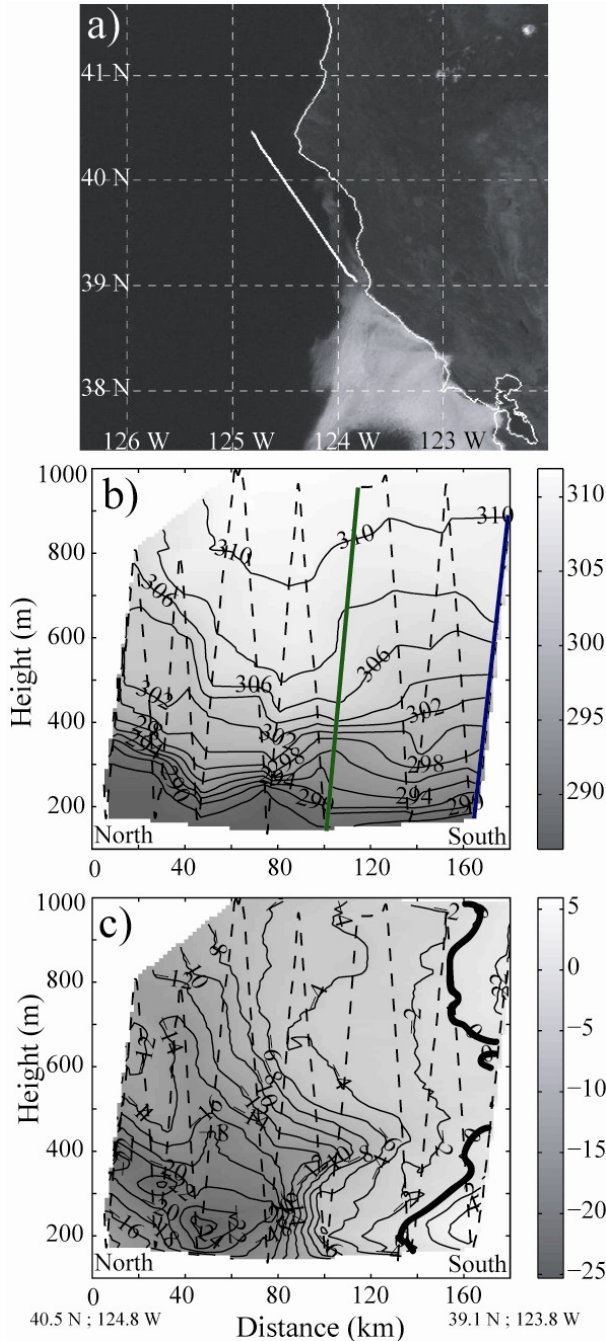


Fig. 8: Sawtooth leg from 2256 to 2339 UTC 23 June 2006 showing (a) the visible satellite image at 2315 UTC overlaid with flight track, (b) potential temperature (K, solid and grayscale), and (c) alongshore wind speed (m s^{-1} , solid and grayscale). Bold line indicates zero contour and the dashed line is the flight track.

marked by changes in temperature and wind. The temperature decreases into the wind reversal layer by ~ 3 C, while the dew point increases by about a degree, Fig. 4c. This depicts the warm, dry air offshore outside the surge layer and the cool, moist air near shore inside the surge layer. Also,

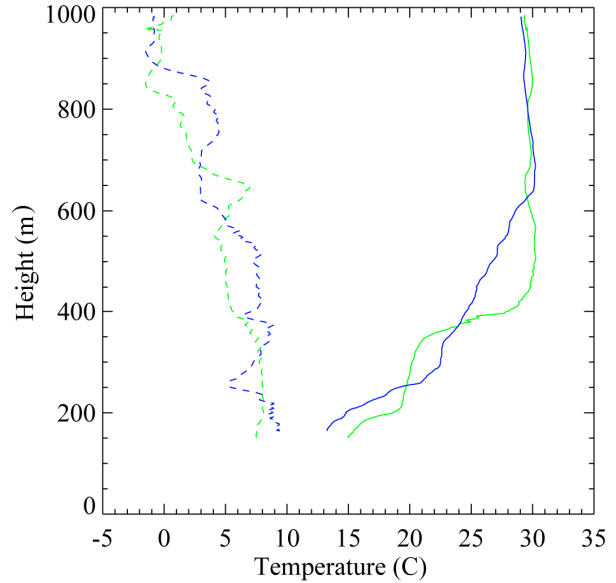


Fig. 9: Profiles of temperature (C, solid) and dewpoint temperature (C, dashed) from the last sawtooth leg. Locations of the middle (green) and south (blue) locations are indicated Fig. 8.

note the small scale fluctuations of temperature between 35 km and 65 km. These are most likely due to temperature fluctuations associated with the small scale cloud structure since this leg is flown near cloud-top. The wind components are shown in Fig. 6d. The CJ weakens steadily toward the shore until it transitions from the northeast to a nearly constant southerly alongshore wind of 4 m s^{-1} in the wind reversal layer. Also, only a slight offshore component of 1 m s^{-1} is present within the wind reversal layer.

Two sawtooth legs, which are along the same track located south of the CTWR head and coming to within 10 km of the coast, examine the cross-shore variation of the MBL, Fig. 7a. The potential temperature contours, Figs. 7b and 7c, show little change in the MBL depth or inversion layer, implying little damming at this time and location. The interpolated cross-shore PGF from both legs is nearly zero throughout the CTWR layer. The cross-shore wind component (not shown) was calm for both of these legs. From these legs and the previous cross-shore isobaric leg, little evidence of cross-shore PGF is indicated at this time and location. Conversely, the alongshore legs do suggest a significant alongshore PGF component. The wind is light in the cross-shore direction within the wind reversal layer. In contrast, the alongshore wind is significant. Since both the PGF and the wind is primarily alongshore, this indicates that alongshore, down-gradient flow

dominates and that the wind is extremely ageostrophic.

The last sawtooth leg on 23 June was an alongshore sawtooth pattern that again sampled the vertical structure of the MBL but further to the north than the first leg, Fig. 8a. Striking changes were observed during this leg. The MBL is deep, well-mixed, and strongly capped near Cape Mendocino, which results from the interaction of the northerly CJ with the terrain. The inversion height decreases substantially into Shelter Cove to the south, and the associated CJ also lowers and increases slightly, which has been previously documented by Rahn and Parish (2007). This strong CJ encounters the region affected by the southerly surge near the center of the leg creating a large gradient in the alongshore wind speed of nearly 14 m s^{-1} over 20 km, an alongshore convergence component of $7 \times 10^{-4} \text{ s}^{-1}$. This is unlikely balanced by cross-shore divergence, and is confirmed by the spreading of the isentropes collocated with this convergence zone showing clear dynamic destabilization. Unlike the single strong inversion capping the MBL in the north, there are really two inversion layers near the center of the leg due to the convergence occurring within the inversion layer.

This is illustrated quite readily in the individual soundings, Fig. 9. The inversion base heights at the center of the leg (green) are near 375 m and 175 m with a more isothermal layer between them. The sounding in the south (blue) shows that the low-level inversion deepens and cools, remaining fairly consistent, while the residual inversion layer above becomes less defined to the south. The shallow cold pool of the CTWR may be associated with this lower inversion and, as shown previously, deepen even further to the south. This suggests that the lower inversion may be controlled predominately by this enhanced convergence aloft near the head of the cloud layer, but dominated by the cloud-top cooling further to the south. It is important to note that the processes in this shallow layer are difficult to simulate, even with a fairly high vertical resolution. For example, the observed convergence occurs mainly in the lowest 400 m and the isothermal layer is only $\sim 150 \text{ m}$ thick.

4. SUMMARY AND CONCLUSIONS

These observations reveal several important features associated with this CTWR event. It is acknowledged that the observations from this case study are influenced by the terrain during these flights and may have evolved from its initiation phase, but they nevertheless still provide

important information. The MBL as indicated by the potential temperature and the cloud layer as measured by the WCR both become deeper to the south. The cloud layer is characterized by a shallow fog that deepens steadily to the south. Evidence of drizzle within this layer is seen in the WCR reflectivity. There is a significant density difference alongshore with cooler air in the south. This cooling associated with the CTWR is verified by the buoy data, which also indicates a concurrent warming of the water temperature as the upwelling is diminished. This leads to the air temperature being cooler than the water temperature after the reversal has passed.

A PGF directed northward is present at the head of the CTWR. The strength of the associated onshore geostrophic wind is $2\text{-}8 \text{ m s}^{-1}$. There is no significant PGF directed normal to the coast within the CTWR. Also, there are no large changes in the MBL depth or characteristics cross-shore that would be associated with significant damming against topography. This is confirmed by several cross-shore legs taken over this day reaching as near as 10 km to the coast. The wind is orientated primarily alongshore with only weak wind cross-shore. These observations indicate that an alongshore, down-gradient flow dominates within the CTWR region. This is in contrast to the region outside of the CTWR region to the west which represents the typical summertime northerly CJ.

The final leg indicates an area of strong convergence in the alongshore component that is confirmed by the dynamic destabilization within the inversion layer. This establishes two inversions with a more isothermal region between them where the majority of the convergence has taken place. The residual inversion that is above the area of convergence tends to diminish to the south, while the lower inversion is still well defined and deepens to the south.

5. REFERENCES

- Burk, S. and W. Thompson, 1996: The summertime low-level jet and marine boundary layer structure along the California Coast. *Mon. Wea. Rev.*, **124**, 668-686.
- Burk, S. and W. Thompson, 2004: Mesoscale eddy formation and shock features associated with a coastally trapped disturbance. *Mon. Wea. Rev.*, **132**, 2204-2223.
- Leon, D., G. Vali, and M. Lothon, 2006: Dual-Doppler analysis in a single plane from an

airborne platform. *J. Atmos. Oceanic Technol.*, **23**, 3-22.

Mass, C. F., and N. Bond, 1996: Coastally trapped wind reversals along the west coast during the warm season. Part II: Synoptic evolution. *Mon. Wea. Rev.*, **124**, 446-461.

Nuss, W. A., and Coauthors, 2000: Coastally trapped wind reversals: Progress toward understanding. *Bull. Amer. Meteor. Soc.*, **81**, 719-743.

Nuss, W. A., 2007: Synoptic-scale structure and character of coastally trapped wind reversals. *Mon. Wea. Rev.*, **135**, 60-81.

Parish T. R., Burkhart M. D., and Rodi A. R., 2007: Determination of the horizontal pressure gradient force using global positioning system on board an instrumented aircraft. *J. Atmos. Oceanic Technol.*, **24**, 521-528.

Rahn, D. A., and T. R. Parish, 2007: Diagnosis of the Forcing and Structure of the Coastal Jet near Cape Mendocino Using In Situ Observations and Numerical Simulations. *J. Appl. Meteor. Climatol.*, in press.

Ralph, F. M., L. Armi, J. M. Bane, C. E. Dorman, W. D. Neff, P. J. Neiman, W. A. Nuss, and P.O.G. Persson, 1998: Observations and analysis of the 10-11 June 1994 coastally trapped disturbance. *Mon. Wea. Rev.*, **126**, 2435-2465.